Journal of Magnetic Resonance **148,** 73–77 (2001)
doi:10.1006/jmre.2000.2208, available online at http://www.idealibrary.com on IDEAL®

Measurement of the Principal Values of the Anisotropic Diffusion Tensor in an Unoriented Sample by Exploiting the Chemical Shift Anisotropy: ^{19}F PGSE NMR with Homonuclear Decoupling

S. V. Dvinskikh[1] and I. Furó[2]

Division of Physical Chemistry, Department of Chemistry, Royal Institute of Technology, SE-10044 Stockholm, Sweden

Received May 8, 2000; revised August 16, 2000

NMR methods (S. V. Dvinskikh *et al., J. Magn. Reson.* 142, 102–110 (2000) and S. V. Dvinskikh and I. Furó, *J. Magn. Reson.* 144, 142–149 (2000)) that combine PGSE with dipolar decoupling are extended to polycrystalline solids and unoriented liquid crystals. Decoupling suppresses dipolar dephasing not only during the gradient pulses but also under signal acquisition so that the detected spectral shape is dominated by the chemical shift tensor of the selected nucleus. The decay of the spectral intensity at different positions in the powder spectrum provides the diffusion coefficient in sample regions with their crystal axes oriented differently with respect to the direction of the field gradient. Hence, one can obtain the principal values of the diffusion tensor. The method is demonstrated by ^{19}F PGSE NMR with homonuclear decoupling in a lyotropic lamellar liquid crystal.

Key Words: **PGSE NMR; homonuclear dipolar decoupling; anisotropic diffusion; liquid crystal; polycrystalline sample.**

INTRODUCTION

Recently, we presented new pulsed-field-gradient spin-echo (PGSE) NMR methods for measuring the diffusion coefficient in anisotropic systems (i.e., other than isotropic liquids) with nonvanishing dipolar coupling (*1, 2*). The methods, which apply heteronuclear (*1*) or homonuclear (*2*) dipolar decoupling, can be used to measure anisotropic diffusion provided that the investigated sample is oriented homogeneously (single crystals or oriented liquid crystals) and the gradient direction relative to the sample orientation can be varied. For many materials, however, it is difficult to obtain a homogeneously oriented sample. Examples are highly viscous thermotropic smectic or lyotropic lamellar liquid crystals.

Measuring the anisotropic diffusion (*3, 4*) in unoriented materials (henceforth referred to as powders) may proceed on two avenues. The first and preferable option is available if the diffusing species presents the spectroscopist with nuclei that have dominant anisotropic spin interactions, such as the quadrupole coupling for $I > \frac{1}{2}$ nuclei. In that case, one obtains the so-called powder spectrum (*5, 6*) where domains of different orientations give rise to signal at different frequencies. By recording the variation of the diffusion damping along the spectrum one may obtain accurate anisotropic diffusion data. Until now, this approach has been pursued in ^{2}H PGSE NMR of water in some anisotropic systems (*7*). Note that for quadrupole broadened spectra, the quadrupole echo must replace the spin echo in the PGSE pulse sequence (*7–9*). A similar approach could be applied to the dipolar powder spectra of isolated few-spin systems.

The other option has been pursued for spin $I = \frac{1}{2}$ nuclei without significant anisotropic couplings such as ^{1}H. In that case, signal from domains with different orientations contribute to the same spectral peak. The resulting diffusion decay, which is a composite of Gaussian decays with different diffusion coefficients, is apparently non-Gaussian in a conventional PGSE experiment (*10–13*). The appearance of this decay also depends on the diffusion time Δ. The diffusion tensor elements could, in principle, be deconvoluted from this composite decay. However, as in any other deconvolution problem (*14*), the result is rather sensitive, for example, to the spectral noise and can therefore seldom be trusted as a source of accurate quantitative data. Here we present a way by which anisotropic diffusion can be accurately measured on suitable spin $I = \frac{1}{2}$ nuclei in powders. The method exploits the orientational dependence of the resonance frequency caused by chemical shift anisotropy (CSA). To uncover this, dipolar decoupling is used. The method is demonstrated by ^{19}F PGSE NMR that is combined with homonuclear decoupling in the lamellar phase of the lyotropic mixture of cesium perfluorooctanoate (CsPFO) and water (*15*).

METHOD

The method is based on a modification of the PGSE pulse sequences (*1, 2*) that were originally designed to study diffusion in homogeneously oriented samples with nonvanishing dipolar couplings. They use dipolar decoupling to suppress the

[1] On leave from the Institute of Physics, St. Petersburg State University, 198904 St. Petersburg, Russia.

[2] To whom correspondence should be addressed. Fax: +46 8 7908207. E-mail: ifuro@physchem.kth.se.

1090-7807/01 $35.00

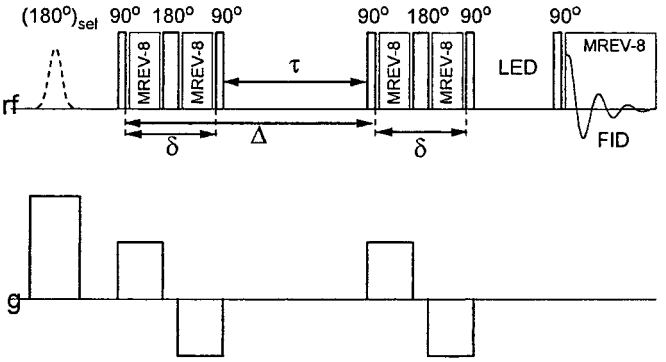

FIG. 1. ^{19}F PGSE NMR combined with MREV-8 homonuclear dipolar decoupling and slice selection. Bipolar gradient pulses (*16*) and a LED (*30*) period are included in the pulse sequence. Acquisition is performed in the presence of homonuclear decoupling. The selective inversion pulse is absent in every second scan and subsequent FIDs are subtracted.

dipolar dephasing during the gradient encoding and decoding periods δ. Since the decoupling is applied in the presence of a strong magnetic field gradient, the decoupling efficiency varies with the gradient strength. The artifact introduced by this feature is suppressed by slice selection. In the original homonuclear pulse sequence (*2*) there was no decoupling during the signal acquisition, primarily to limit sample heating. While this is not a problem in suitably oriented samples (all signal arises from regions of the same orientation with respect to the applied field gradient), in polycrystalline samples the strong dipolar broadening obscures the orientation dependence. If, however, the signal can be acquired under homonuclear decoupling, the dipolar broadening disappears, exposing the powder spectrum caused by CSA. The corresponding pulse sequence is shown in Fig. 1. Another difference, compared to Refs. (*1, 2*), is the use of bipolar gradient pulses which suppress artifacts caused by the cross-relaxation process during the period τ (*16*).

The diffusion experiment proceeds by recording the variation of the signal intensity on increasing the diffusion delay Δ. In general, the resulting damping of the signal for a particular domain depends on the relative orientation of the second-rank diffusion tensor **D** (set by the orientation of the domain) to the direction of the gradient **g** (set by the applied gradient coil). This is usually formulated by replacing the classical g^2D term in the Stejskal–Tanner expression (*17, 18*) by the bilinear form **gDg** (*3, 4, 19*) that yields

$$S(\Delta) \sim \exp(-R \cdot \Delta), \qquad [1a]$$

with

$$R = (\gamma s \delta)^2 \mathbf{gDg} + 1/T_1, \qquad [1b]$$

where s is the scaling factor of the decoupling sequence (*6*) and γ is the magnetogyric ratio. (We neglect the orientation-dependence of the scaling factor and relaxation time T_1.)

In the general case, the diffusion tensor **D** is characterized by its three principal values D_i, $i = \alpha, \beta, \gamma$. In powder samples, these individual principal values are only accessible if the exploited coupling tensor, quadrupole or CSA, is significantly nonaxially symmetric. Below, we concentrate on the formally simpler case of uniaxial symmetry that is more relevant for liquid crystals. In that case, the diffusion tensor has two principal values denoted by $D_\parallel$ and $D_\perp$ and the axis of symmetry coincides with the direction associated with $D_\parallel$. Although not necessarily the case, a uniaxial symmetry of **D** in liquid crystals is usually accompanied by uniaxial quadrupole and CSA coupling tensors. Hence, the orientation of a particular domain with respect to the magnetic field $\mathbf{B}_0$ is sufficiently characterized by a single angle θ between the phase director **P** (*20*) within the domain and $\mathbf{B}_0$.

If **g** is set parallel to $\mathbf{B}_0$, θ provides the relative orientation of both the diffusion and the coupling tensors with respect to $\mathbf{B}_0$. Hence, the bilinear form **gDg** in Eq. [1b] can be simplified to $g^2D(\theta)$ (*3*) with

$$D(\theta) = D_\parallel \cos^2\theta + D_\perp \sin^2\theta. \qquad [2]$$

Provided that the diffusion distance $d = (6D_{\max}\Delta)^{1/2}$ with $D_{\max}$ denoting the faster of the principal values is small compared to the domain size, the obtained spectra can be straightforwardly analyzed to provide the principal values of the diffusion tensor. In particular, the intensity decays measured at the spectral edges provide directly $D_\parallel$ and $D_\perp$.

On the other hand, if **g** is set to an arbitrary angle with respect to $\mathbf{B}_0$, the domains that are oriented at θ with respect to $\mathbf{B}_0$ contribute to the powder spectrum at the same frequency but the angle between their phase director **P** and **g** varies. Therefore, there is a distribution of **gDg** among those domains and such an experimental setup results in a composite decay that is generally non-Gaussian and is therefore more difficult to analyze.

RESULTS AND DISCUSSION

The homonuclear-dipolar-decoupled ^{19}F NMR powder spectrum in the lamellar phase of the CsPFO–D_2O mixture, recorded at 188 MHz and at 298 K, is shown in Fig. 2a. The spectrum is a superposition of the axially symmetric CSA powder patterns (*6*) that correspond to different fluorine positions within the surfactant molecule. The CSA tensors are reduced with respect to their instantaneous molecular values both by molecular motions (*1, 21*) and scaling by the homonuclear decoupling (*2*). The line positions in the spectrum of an oriented sample in Fig. 2b (with the phase director parallel to $\mathbf{B}_0$) coincide with the high field edges of individual powder patterns in Fig. 2a. The spectrum is assigned as previously communicated (*22*).

First, $D_\parallel$ and $D_\perp$ were obtained in a homogeneously *oriented* lamellar liquid crystal prepared by cooling the sample from the

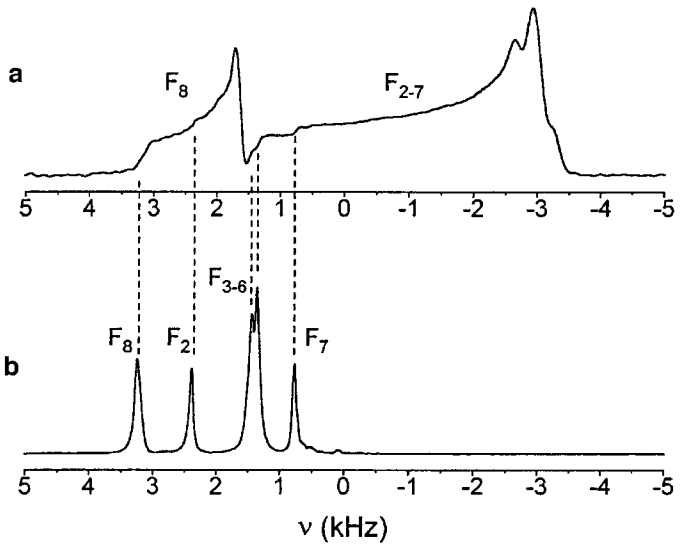

FIG. 2. ^{19}F homonuclear-decoupled NMR spectra of CsPFO/D_2O (at 40 wt%) in the lamellar phase at 298 K. (a) Sample with random domain orientation. (b) Homogeneously oriented sample with its director parallel to the static magnetic field. MREV-8 homonuclear decoupling with 2.5-μs 90° pulse length and 84-μs cycle time was applied to obtain both spectra. Note that the frequency scale is not corrected by the scaling factor s ($\approx$0.5) of the decoupling sequence. The fluorines that contribute to the spectrum are numbered by the corresponding carbon position in the surfactant molecule: the F_2 fluorines reside on the difluoromethylene group closest to the carboxylate carbon and the F_8 fluorines reside in the terminal trifluoromethyl group.

adjacent nematic phase into the lamellar phase within the magnetic field (*23*). The experiment performed as previously described (*1*, *2*) provided us with the data presented in Fig. 3, from which least-square fits yield $D_{\parallel} = (2.5 \pm 0.3) \cdot 10^{-12}$ m^2/s and $D_{\perp} = (5.4 \pm 0.2) \cdot 10^{-11}$ m^2/s, corresponding to the

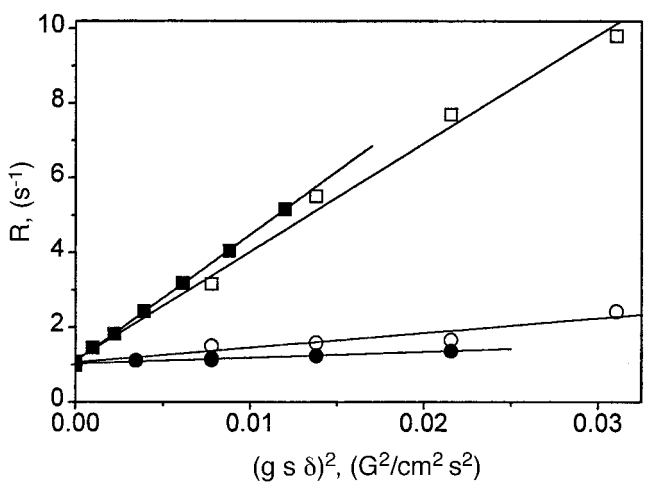

FIG. 3. The variation of the decay constant R (see Eq. [1b]) on increasing gradient strength g and/or duration δ. The effective gradient strength is provided by the scaling factor s of the homonuclear decoupling (*6*). Full and open symbols are data from oriented and unoriented samples, respectively, providing, via Eq. [1b], $D(\theta)$ at $\theta = 0°$ (○, ●) and $\theta = 90°$ (□, ■).

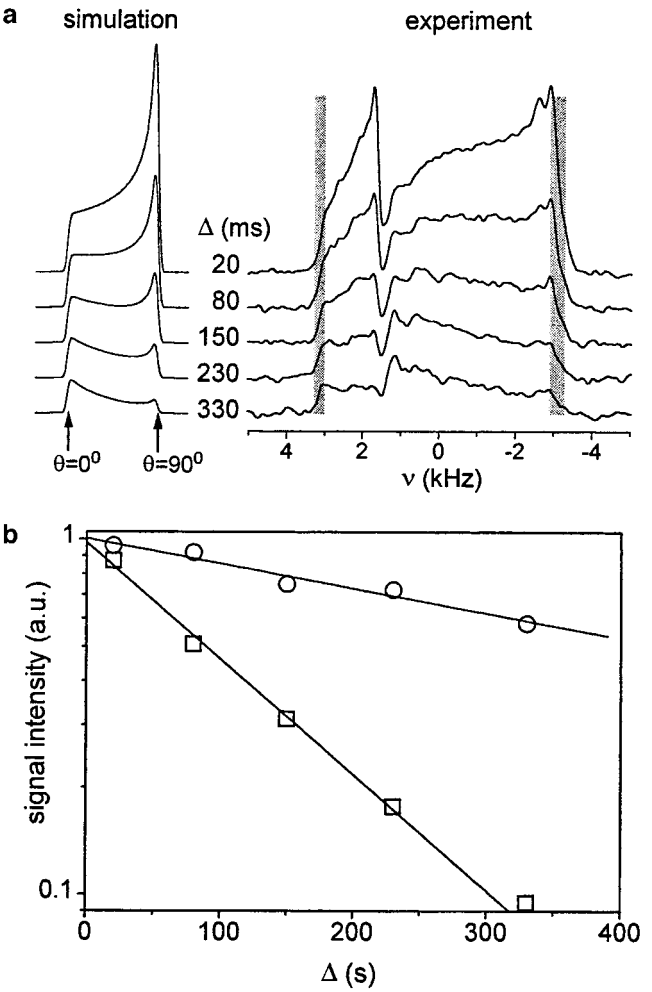

FIG. 4. (a) ^{19}F spectra obtained with the pulse sequence in Fig. 1 at different diffusion times Δ and with gradient strength $g = 190$ G/cm and gradient pulse length $\delta = 1.68$ ms. The gradient is parallel to the static magnetic field $\mathbf{B}_0$. The simulated spectra (left side) are calculated with an axially symmetric CSA tensor with diffusion coefficients $D_{\parallel} = 2.5 \times 10^{-12}$ m^2/s and $D_{\perp} = 5.4 \times 10^{-11}$ m^2/s measured in an oriented sample (see text) and with the longitudinal relaxation time set to $T_1 = 1$ s. (b) The decay of the spectral intensities at the edges with increasing diffusion time Δ (see Fig. 1). The points (○, left edge at 3 kHz corresponding to $\theta = 0°$; □, right edge at -3 kHz corresponding to $\theta = 90°$) are integral intensities from the shadowed regions. The dependence of the fitted (solid line) decay constants on the gradient strength g and duration δ is shown in Fig. 3.

surfactant diffusion perpendicular and parallel to the lamellar bilayers, respectively. The obtained ratio $D_{\perp}/D_{\parallel} \approx 20$ is close to that found for the same surfactant but at a different concentration and temperature (*1*).

Second, $D_{\parallel}$ and $D_{\perp}$ were obtained in an *unoriented* sample prepared by cooling the sample but outside the magnetic field. With the pulse sequence in Fig. 1 and $\mathbf{g}$ parallel to $\mathbf{B}_0$, the spectral shape varies on changing Δ as demonstrated in Fig. 4 for $g = 190$ G/cm. In contrast, no detectable variation of the spectral shape with increasing diffusion time Δ was observed with zero gradient and the experiment yielded an exponential

decay with the time constant $T_1 \approx 1$ s. Using this decay constant and the diffusion coefficients obtained in the oriented sample (see above), we have simulated via Eqs. [1] and [2] the decay of a CSA powder spectrum with increasing Δ. As demonstrated by Fig. 4 there is a qualitative agreement between the experimental and simulated spectra. A quantitative simulation of the spectral shape requires taking into account the anisotropy of the transverse relaxation and the overlap of the individual ^{19}F spectra.

The two principal values of the diffusion tensor can be obtained, however, without spectral simulation. For each individual spectrum of Fig. 4, the intensity at the left edge is contributed by domains with their director parallel to $\mathbf{B}_0$ ($\theta = 0°$), while domains with director orientation perpendicular to $\mathbf{B}_0$ ($\theta = 90°$) contribute to the right edge of each individual spectrum. Hence, $D_\parallel$ and $D_\perp$ can be simply obtained by recording the decay of the respective spectral edges. In our particular spectra with their partial overlap (see Fig. 2), the decay of the left edge of the F_8 powder spectrum provides $D_\parallel$ and the right edge of the composite F_{2-7} powder spectrum provides $D_\perp$. By performing several experiments with gradient strength in the range from zero to 230 G/cm (see data in Fig. 3), the linear dependence of the decay constant R on g^2 (see Eq. [1b]) provides us with $D_\parallel = (6 \pm 1) \cdot 10^{-12}$ m^2/s and $D_\perp = (4.8 \pm 0.4) \cdot 10^{-11}$ m^2/s.

The obtained values of the diffusion coefficient for the fast in-bilayer diffusion $D_\perp$ agree well for oriented and unoriented samples. On the other hand, $D_\parallel$ is overestimated (by a factor of 2) in the measurement performed in the unoriented sample. This can mainly be attributed to the large linewidth ($\approx$150 Hz, caused mainly by inhomogeneous broadening) and the exponential multiplication prior to Fourier transform (50 Hz). Hence, the intensity at the high-frequency edge of the F_8 spectrum is contributed not only by domains with $\theta = 0°$ but also by other ones with an orientation distribution around 0°. With 200 Hz line broadening and about 2 kHz full width (scaled down by homonuclear decoupling (*6*)) of the F_8 powder spectrum, the width of this orientation distribution is more than 10°. $D_\perp$ is less sensitive to this effect since the relative variation of the diffusion coefficient in the vicinity of its maximum value is much smaller and, moreover, the powder spectrum for F_{2-7} is wider. There might also be some influence from exchange of molecules among domains with different orientation. Again, $D_\parallel$ is more sensitive to that process than $D_\perp$. For $\Delta = 100$ ms and $D = 5 \cdot 10^{-11}$ m^2/s, the average diffusion distance is $\langle r^2 \rangle^{1/2} = (6D\Delta)^{1/2} = 5$ μm, which is a plausible size range for domains in lyotropic liquid crystals. ^{19}F 2D exchange experiments (*24*) performed with several mixing times (results not shown) indicate the onset of significant interdomain exchange at around 300 ms. The influence of this process on a diffusion experiment can be reduced by choosing a shorter diffusion time and correspondingly stronger and/or longer gradient pulses.

CONCLUSION

As demonstrated above, the principal values of the anisotropic self diffusion tensor can be measured in polycrystalline samples by a PGSE-type experiment with decoupling during both the gradient pulses and the acquisition period. The method does not require quadrupolar probe nuclei as in previous experiments (*7*). Instead of exploiting the quadrupole coupling, the orientational dependence of the resonance frequency of spin $I = \frac{1}{2}$ nuclei via their chemical shift anisotropy is used to distinguish between domains with different orientation. Therefore, nuclei with substantial chemical shift anisotropy (*6*), like ^{19}F, ^{13}C, and ^{31}P, are the most feasible as a probe. Depending on the source of the dominant dipolar broadening, one can use heteronuclear or homonuclear decoupling, of which the latter option is demonstrated here experimentally. In the present sample, the diffusion anisotropy would also be accessible, albeit in a longer experiment, via the large ^{13}C CSA of the carbonyl carbon (*21*).

If its time scale is comparable with the diffusion time Δ, molecular exchange between domains with different orientation puts a limit on the accuracy of the measured diffusion anisotropy. A short diffusion time might therefore be preferable to use.

EXPERIMENTAL

Cesium perfluorooctanoate was synthesized as described previously (*9*). The liquid crystal sample was produced by mixing CsPFO (40 wt%) with D_2O. The nematic–lamellar phase transition temperature was established to 299 K from the ^{2}H spectrum. The lamellar sample with random director orientation was prepared by cooling the sample through its isotropic and nematic phases outside the magnetic field. Due to the high viscosity of the phase, the sample remains unoriented in the magnetic field for long times (a few days or longer if it is more than 0.5 K away from the nematic–lamellar phase transition). The homogeneously oriented lamellar sample was prepared by cooling the sample from the nematic phase with the sample inside the magnet (4.7 T field strength). The nematic director orients parallel to the external magnetic field and this orientation is kept in the lamellar phase (*23*). The sample orientation was checked by observing the ^{2}H spectrum of D_2O which is a powder pattern and a doublet in polycrystalline and oriented phases, respectively.

The measurements were performed on a Bruker DMX 200 spectrometer, operating at 188 MHz for ^{19}F. We used a home-built gradient probe (*2, 25*). The length of the ^{19}F 90° pulse was 2.5 μs (with 300-W irradiation power). The gradient coils were driven by a Bruker BAFPA-40 current generator. The gradient strength was calibrated earlier (*1*). The Gaussian-shaped selective inversion pulse (47 μs) of 30 kHz nominal bandwidth was truncated at 2% of its peak amplitude. The following phase cycle was applied: first 90° pulse $2(+x)$, $2(+y)$; second and

third 90° pulses $+x$, $2(+y)$, $-x$; fourth and fifth 90° pulses $2(+x)$, $2(+y)$; receiver $2(-x)$, $2(-y)$. The phases of the 180° pulses coincided with the phase of first 90° pulse. Each cycle is repeated twice with and without selective inversion pulse (with phase $+x$) and the receiver phase is inverted for subsequent cycles. The pulse phases in the MREV-8 (*26, 27*) sequence were alternated between $(+x, +y, -y, -x, -x, +y, -y, +x)$ and $(+x, -y, +y, -x, -x, -y, +y, +x)$ after each eight scans. The MREV-8 sequence was sandwiched (*28, 29*) as $(45°)_{-y}$–(MREV-8)–$(45°)_{+y}$. The scaling factor of the MREV-8 sequence was calibrated depending on frequency offset as described earlier (*2*). The value $s = 0.46$ averaged in the frequency offset range ± 15 kHz was used for calculating the diffusion coefficient via Eq. [1]. The delay δ was set to 1.68 ms, which corresponds to 28 MREV-8 cycles of 60 μs.

A total of 256 transients (preceded by 16 dummy scans) were accumulated for each individual spectrum of the diffusion experiment. The average temperature was regulated with an accuracy of 0.1 K by the Bruker BVT-3000 unit. A recycle delay of 16 s (much longer than required for full spin relaxation) was used to allow for sufficient heat dissipation from decoupling. Heating effects amount to about 0.4 K average temperature spread and about 0.4 K average temperature shift.

ACKNOWLEDGMENTS

This work was supported by the Swedish Natural Science (NFR) and Engineering Science (TFR) Research Councils and the Carl Trygger Foundation. S.V.D. thanks the Wenner-Gren Foundations for a scholarship.

REFERENCES

1. S. V. Dvinskikh, R. Sitnikov, and I. Furó, ^{13}C PGSE NMR experiment with heteronuclear dipolar decoupling to measure diffusion in liquid crystals and solids, *J. Magn. Reson.* **142,** 102–110 (2000).
2. S. V. Dvinskikh and I. Furó, Combining PGSE NMR with homonuclear dipolar decoupling, *J. Magn. Reson.* **144,** 142–149 (2000).
3. P. T. Callaghan, "Principles of Nuclear Magnetic Resonance Microscopy," Clarendon Press, Oxford, 1991.
4. W. S. Price, Pulsed-field gradient nuclear magnetic resonance as a tool for studying translational diffusion: Part I. Basic theory, *Concepts Magn. Reson.* **9,** 299–336 (1997).
5. A. Abragam, "The Principles of Nuclear Magnetism," Clarendon, Oxford, 1961.
6. M. Mehring, "Principles of High Resolution NMR in Solids," Springer, Berlin, 1983.
7. P. T. Callaghan, M. A. Le Gros, and D. N. Pinder, The measurement of diffusion using deuterium pulsed field gradient nuclear magnetic resonance, *J. Chem. Phys.* **79,** 6372–6381 (1983).
8. I. Furó and B. Halle, 2D quadrupolar echo spectroscopy with coherence selection and optimized pulse angle, *J. Magn. Reson.* **98,** 388–407 (1992).
9. H. Jóhannesson, I. Furó, and B. Halle, Orientational order and micelle size in the nematic phase of the cesium pentadecafluorooctanoate–water system from the anisotropic self-diffusion of water, *Phys. Rev. E* **53,** 4904–4917 (1996).
10. P. T. Callaghan, K. W. Jolley, and J. Lelievre, Diffusion of water in the endosperm tissue of wheat grains as studied by pulsed field gradient nuclear magnetic resonance, *Biophys. J.* **28,** 133–141 (1979).
11. P. T. Callaghan and O. Söderman, Examination of the lamellar phase of Aerosol OT/water using pulsed field gradient nuclear magnetic resonance, *J. Phys. Chem.* **87,** 1737 (1983).
12. F. D. Blum, A. S. Padmanabhan, and R. Mohebbi, Self-diffusion of water in polycrystalline smectic liquid crystals, *Langmuir* **1,** 127–131 (1985).
13. L. Coppola, C. L. Mesa, G. A. Ranieri, and M. Terenzi, Analysis of water self-diffusion in polycrystalline lamellar systems by pulsed field gradient nuclear magnetic resonance experiments, *J. Chem. Phys.* **98,** 5087–5090 (1993).
14. A. A. Istratov and O. F. Vyvenko, Exponential analysis in physical phenomena, *Rev. Sci. Instr.* **70,** 1233–1257 (1999).
15. N. Boden, S. A. Corne, and K. W. Jolley, Lyotropic mesomorphism of the cesium pentadecafluorooctanoate/water system: High-resolution phase diagram, *J. Phys. Chem.* **91,** 4092–4105 (1987).
16. S. V. Dvinskikh and I. Furó, Cross-relaxation effects in stimulated-echo-type PGSE NMR experiments by bipolar and monopolar gradient pulses, *J. Magn. Reson.***146,** 283–289 (2000).
17. E. O. Stejskal and J. E. Tanner, Spin diffusion measurements: Spin echoes in the presence of a time-dependent field gradient, *J. Chem. Phys.* **42,** 288–292 (1965).
18. J. E. Tanner, Use of the stimulated echo in NMR diffusion studies, *J. Chem. Phys.* **52,** 2523–2526 (1970).
19. E. O. Stejskal, Use of spin echoes in a pulsed magnetic-field gradient to study anisotropic, restricted diffusion and flow, *J. Chem. Phys.* **43,** 3597–3603 (1965).
20. P. G. de Gennes and J. Prost, "The Physics of Liquid Crystals," Clarendon, Oxford, 1993.
21. S. V. Dvinskikh and I. Furó, Order parameter profile of perfluorinated chains in a lamellar phase, *Langmuir* **16,** 2962–2967 (2000).
22. R. Raulet, I. Furó, J. Brondeau, B. Diter, and D. Canet, Water–surfactant contact studied by ^{19}F–^{1}H heteronuclear Overhauser effect spectroscopy, *J. Magn. Reson.* **133,** 324–329 (1998).
23. N. Boden, G. R. Hedwig, M. C. Holmes, K. W. Jolley, and D. Parker, Anomalous effects in experiments on monodomain nematic and lamellar phases of the caesium pentadecafluoroocatnoate(CsPFO)/water system, *Liq. Cryst.* **11,** 311–324 (1992).
24. K. Schmidt-Rohr and H. W. Spiess, "Multidimensional Solid-State NMR and Polymers," Academic Press, London, 1994.
25. I. Furó and H. Jóhannesson, Accurate anisotropic water diffusion measurements in liquid crystals, *J. Magn. Reson. A* **119,** 15–21 (1996).
26. P. Mansfield, Symmetrized pulse sequences in high resolution NMR in solids, *J. Phys. C* **4,** 1444–1447 (1971).
27. W. K. Rhim, D. D. Elleman, and R. W. Vaughan, Analysis of multiple pulse NMR in solids, *J. Chem. Phys.* **59,** 3740–3749 (1973).
28. T. M. Barbara and L. Baltusis, Phase-cycled, multiple-window-acquisition, multiple-pulse NMR spectroscopy, *J. Magn. Reson. A* **106,** 182–187 (1994).
29. H. Cho, Off-resonance multiple-pulse dynamics in solid-state NMR spectroscopy: A revised coherent averaging theory analysis, *J. Magn. Reson.* **141,** 164–179 (1999).
30. S. J. Gibbs and C. S. Johnson, A PFG NMR experiment for accurate diffusion and flow studies in the presence of eddy currents, *J. Magn. Reson.* **93,** 395–402 (1991).